Climbing end image algorithm to locate transition states

Climbing end image algorithm to locate transition states

Toshio Asada*[†,‡], Nozomi Sawada[†], Mamoru Haruta[†], and Shiro Koseki[†,‡]

[†]Department of Chemistry, Graduate School of Science, Osaka Prefecture University, 1-1 Gakuen-cho, Naka-ku, Sakai 599-8531, Japan.

[‡]The Research Institute for Molecular Electronic Devices (RIMED), Osaka Prefecture University, 1-1 Gakuen-cho, Naka-ku, Sakai 599-8531, Japan.

Abstract

A climbing end image algorithm is proposed to locate transition state structures based on the nudged-elastic-band method. According to this algorithm, all intermediate structures, known as images in the nudged-elastic-band method, can climb the potential energy surface along the reaction path to the transition state. The number of images can be reduced because all images are located in the limited transition state region. This method was applied to the simplified Wittig reaction, and two transition state structures were successfully found with high reliability.

Keywords:

climbing end image algorithm, nudged elastic band, transition state optimization, Witting reaction

1. Introduction

Structural optimizations of transition states (TSs) are necessary to understand the detailed mechanisms of a wide range of chemical reactions. To obtain TS structures, the second derivative of the potential energy surface with respect to the nuclear coordinates, known as a Hessian, is usually useful if available for application to efficient optimization algorithms, such as Newton's method [1]. However, it is sometimes difficult to obtain analytical Hessians, and a considerable computational time is required to evaluate numerical or pseudo Hessians using methods such as the Broyden–Fletcher–Goldfarb–Shanno method [2]. In addition, although the free energy gradients [3–6] can be obtained using molecular dynamics simulations in a solvent, it is also difficult to obtain reliable free energy Hessians because of thermal fluctuations. Moreover, according to the conventional optimization algorithm, an initial structure close to the TS should be prepared, although no reaction information is available. To overcome this difficulty, alternative methods to address the TS structure have been proposed. The chain of state methods, such as the nudged elastic band (NEB) [7–9] and string [10,11], were proposed to be powerful approaches for optimizing the minimum energy path (MEP) on the energy surface using discretized intermediate structures (images) between the reactant and the product. According to these approaches, the number of images should be increased to improve the reliability, as the discretized structures represent the MEP. The improved method, adaptive NEB (ANEB), was proposed by Maragakis et al. [12] to reduce the number of images to obtain the TS. The ANEB method can reduce the number of images by cutting the reaction path and adding the new images by interpolation repeatedly to calculate only the limited region near the TS. It is possible to increase the density of images. However, the interpolated images are not guaranteed to be placed on the MEP unless the images are already dense near the TS, though it depends on the system.

In this paper, an efficient algorithm named “climbing end image (CEI)” is proposed to obtain the TS structures. Based on this algorithm, all images climb the potential energy surface along the MEP towards the TS structures between a given reactant and a product. The proposed algorithm can reduce the number of images without reducing the reliability of the

optimized TS structures. We have already implemented this algorithm in the GAMESS program [13]. Detailed discussions are provided on the application of the CEI algorithm to address the TS structures in the simple Wittig reaction [14,15].

2. Computational Method

2.1 CEI algorithm

Based on the NEB method, the reaction path can be represented by a chain of states, in which a given number of equally separated images are interpolated between the reactant and product structures. Although the simplest linear interpolation algorithm can be used to determine the structure of images, it sometimes causes collisions of atoms in some images. To avoid such difficulties, a combination of the image-dependent pair potential (IDPP) [16] and the NEB methods is adapted in this study to prepare the initial structures. The combined algorithm can reasonably determine the initial reaction pathway, reflecting suitable geometrical changes for the chemical reaction.

According to the NEB algorithm, the structure of the *i*-th (i = 1–N) image can be optimized to align the MEP using modified forces, $\mathbf{F}_i'$, with respect to the perpendicular, $\mathbf{F}_i^{\perp}$, and the parallel components, $\mathbf{F}_i^{//}$, of forces acting on the *i*-th image, $\mathbf{F}_i$.

$$\mathbf{F}_i' = \mathbf{F}_i^{\perp} + \mathbf{F}_i^{//} = \begin{cases} \left[\mathbf{F}_i - \left(\mathbf{F}_i \cdot \hat{\boldsymbol{\tau}}_i\right)\hat{\boldsymbol{\tau}}_i\right] + k'\left[\left|\mathbf{x}_{i+1} - \mathbf{x}_i\right| - \left|\mathbf{x}_i - \mathbf{x}_{i-1}\right|\right]\hat{\boldsymbol{\tau}}_i & (i \neq 1, N) \\ \left[\mathbf{F}_i - \left(\mathbf{F}_i \cdot \hat{\boldsymbol{\tau}}_i\right)\hat{\boldsymbol{\tau}}_i\right] & (i = 1, N) \end{cases}, \quad (1)$$

where $\hat{\boldsymbol{\tau}}_i$ is a tangent vector conventionally approximated by the parallel direction of the displacement vector of atoms originating from the (*i-1*)-th to the (*i+1*)-th images, because the exact tangent vector cannot be obtained during optimization procedures [12,17]. In the conventional NEB method [9], $\hat{\boldsymbol{\tau}}_i$ is represented as

$$\hat{\boldsymbol{\tau}}_i = \frac{\mathbf{x}_{i+1} - \mathbf{x}_{i-1}}{\left|\mathbf{x}_{i+1} - \mathbf{x}_{i-1}\right|}. \quad (2)$$

$\mathbf{F}_i^{//}$ is an artificial force used to maintain equally separations between neighboring images.

When the distance (2-norm) between neighboring images is sufficiently short, $\hat{\boldsymbol{\tau}}_i$ is reliable, as shown in Scheme 1.

This is because the derivative at a given coordinate x can be obtained by the simple central difference approximation as

$$f'(x) = \lim_{h \to 0} \frac{f(x+h) - f(x-h)}{2h} \quad , \tag{3}$$

where h is the small difference of the coordinate from x. This means that equally separations and short distances between images are very important to obtain the reliable tangent vector $\hat{\boldsymbol{\tau}}_i$.

While terminal images of $i = 1 \text{ and } N$, denoted as "end images", do not move toward lower energy in principle because the parallel component of forces is eliminated in Eq.(1), the end images tend to move toward lower energy on the potential surface in the actual calculation due to the unreliability of $\hat{\boldsymbol{\tau}}_i$.

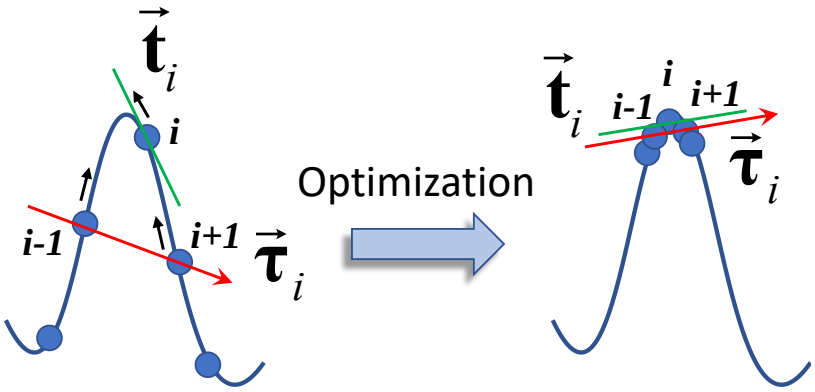

Scheme 1. High density of images at the TS region increases the reliability of the approximated tangent vector τ_i along the reaction path in CEI algorithm. Vectors $\vec{t}_i$ and τ_i are the accurate tangent and approximate tanget vectors at the *i*-th image, respectively.

If only TS structures are of interest, the distance between neighboring images can be reduced if the pathway is limited to the TS region. The modified forces in CEI incorporate the climbing image (CI) algorithm [18] and are defined as follows.

$$\mathbf{F}_{\mathrm{CEI},i}' = \mathbf{F}_i^{\perp} + \mathbf{F}_{\mathrm{CEI},i}^{//}$$

$$= \begin{cases} \left[\mathbf{F}_i - (\mathbf{F}_i \cdot \hat{\boldsymbol{\tau}}_i)\hat{\boldsymbol{\tau}}_i\right] + k'\left[|\mathbf{x}_{i+1} - \mathbf{x}_i| - |\mathbf{x}_i - \mathbf{x}_{i-1}|\right]\hat{\boldsymbol{\tau}}_i & (i \neq 1, N, imax) \\ \left[\mathbf{F}_1 - (\mathbf{F}_i \cdot \hat{\boldsymbol{\tau}}_1)\hat{\boldsymbol{\tau}}_1\right] + k''\left[|\mathbf{x}_2 - \mathbf{x}_1| - \lambda d_{ave}^0\right]\hat{\boldsymbol{\tau}}_1 & (i = 1) \\ \left[\mathbf{F}_N - (\mathbf{F}_N \cdot \hat{\boldsymbol{\tau}}_N)\hat{\boldsymbol{\tau}}_N\right] - k''\left[|\mathbf{x}_N - \mathbf{x}_{N-1}| - \lambda d_{ave}^0\right]\hat{\boldsymbol{\tau}}_N & (i = N) \\ \mathbf{F}_{imax} - 2(\mathbf{F}_{imax} \cdot \hat{\boldsymbol{\tau}}_{imax})\hat{\boldsymbol{\tau}}_{imax} & (i = imax) \end{cases} \quad , \tag{4}$$

where *imax* is the image with the highest energy, d_{ave}^0 is the averaged distance between neighboring images in the initial

pathway and λ is a given value to maintain distances between images between 0 and 1.

The tangent vector of the end image are defined as

$$\hat{\boldsymbol{\tau}}_1 = \frac{\mathbf{x}_2 - \mathbf{x}_1}{\left|\mathbf{x}_2 - \mathbf{x}_1\right|}, \tag{5}$$

$$\hat{\boldsymbol{\tau}}_N = \frac{\mathbf{x}_N - \mathbf{x}_{N-1}}{\left|\mathbf{x}_N - \mathbf{x}_{N-1}\right|}. \tag{6}$$

Because this algorithm uses the CI algorithm [18] at the *imax*-th image to climb the potential energy surface towards the TS and the end images also climb the potential surface, all images cluster around the TS along the MEP if λ is set to be small in Eq.(4). In the GAMESS program Δr, which is λd_{ave}^{0}, must be specified to optimize TSs. The constant value of 0.05 was adapted for Δr through the calculations in this study.

2.2 Model system

The CEI algorithm was applied to the simple Wittig reaction, in which alkene is synthesized from ketone and phosphorous ylide, as shown in Fig. 1.

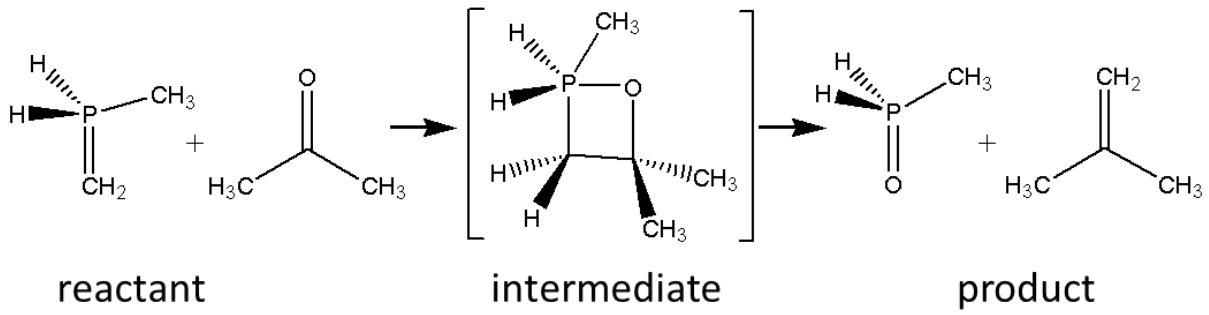

Fig. 1. Wittig reaction.

The reactant and product complexes were fully optimized, and nine structures were interpolated using the IDPP algorithm to prepare the initial reaction path as the chain of states consisted of 11 images. Then, the reaction path was optimized to find TSs using the CI and CEI algorithms proposed in this study, and the characteristic features of the CEI algorithm was discussed. The energies and forces of all structures were calculated using B3LYP functionals including the Grimme's empirical dispersion correction. The basis set used in this study was 6-311++G(d,p). All DFT calculations were performed using the

GAMESS program codes [13].

3. Results and Discussions

The optimized structures of the reactant (1st image) and the product complexes (11th image) are shown in Fig. 2. The initial reaction path was prepared by using the IDPP approach, based on which, structures are continuously displaced from the reactant to the product without conflicting atoms for all interpolated images, as shown in Fig. 3a. The corresponding energy profile was calculated as shown in Fig. 3b; this potential curve had the highest energy of ca. 240 kcal/mol at the 6th image, because the initial reaction pathway was generated by applying the linear interpolation algorithm between the reactant and the product. Then, all images in the initial pathway were optimized for 100 cycles by using the original NEB approach represented in Eq.1. The input file for this optimization by GAMESS is provided in the supplementary material.

During the optimization procedure, the energy at the 6th image decreased to be the intermediate structure IM (Fig. 3b).

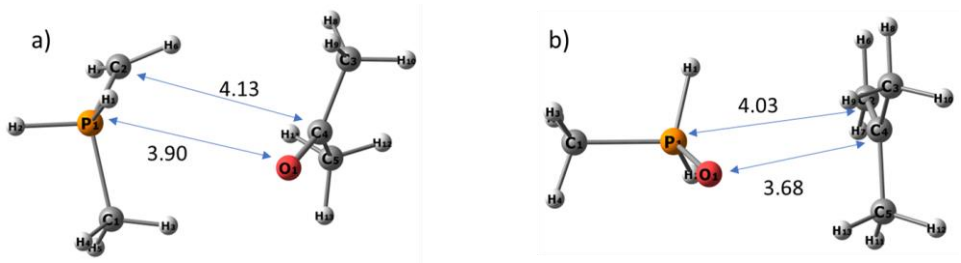

Fig. 2. Optimized structures: a) reactant and b) product. Values are interatomic distances in Å.

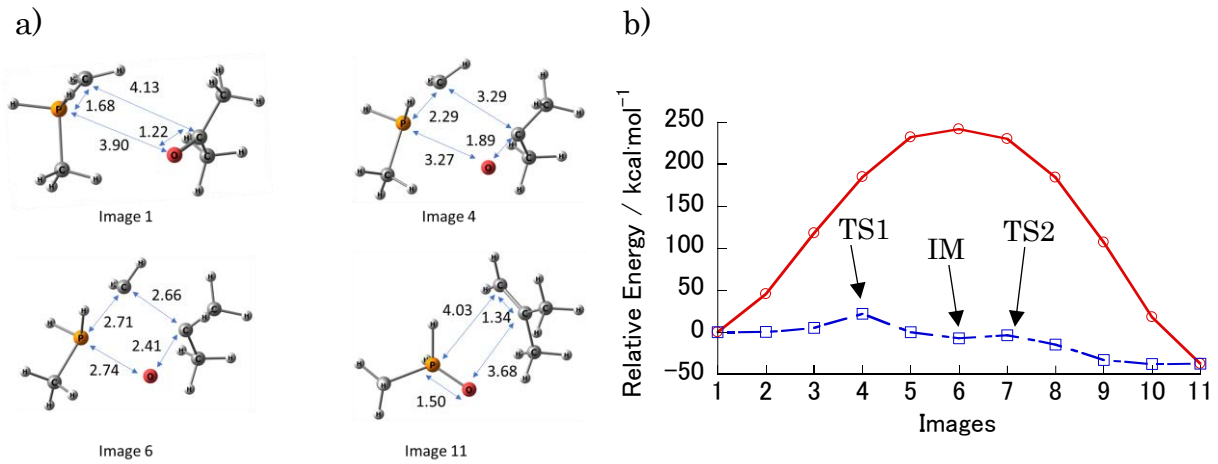

Fig. 3. Initial interpolated structures along the reaction pathway obtained by using IDPP approach. a) The structure of some images and b) the relative energy profile along the initial (solid line) and the optimized (100 cycles) (broken line) reaction paths in kcal/mol.

It should be noted that TS regions and intermediate structures can be predicted along the energy profile if they exist between both end images using the NEB method. In our calculation, two TSs were found at the 4th and 7th images, whose relative energies based on the reactant were +21.9 and -3.5 kcal/mol, respectively. Because these structures were optimized by using the quick-min algorithm [19,20], many optimization cycles were required to obtain the MEP. However, there is no doubt that the implementation of more efficient optimization techniques such as the global L-BFGS or the first inertial relaxation engine[21] can reduce the number of optimization cycles[20] to converge.

As IM was obtained (Fig. 3b), conventional CI and CEI calculations were performed to locate TSs, TS1 between the reactant and IM, and TS2 between IM and the product. For both TS optimizations, 11 images were interpolated to describe each reaction pathway individually. The calculated energy profiles after 100 optimization cycles are shown in Fig. 4. It is clear that all images successfully climbed the potential energy surface toward the TSs by using the CEI approach and not using the CI approach. Thus, the high density of images in the CEI approach should reproduce reliable tangent vectors along the reaction path as optimizations proceeds, by approximation as shown in Eqs. 2, 3, 5 and 6.

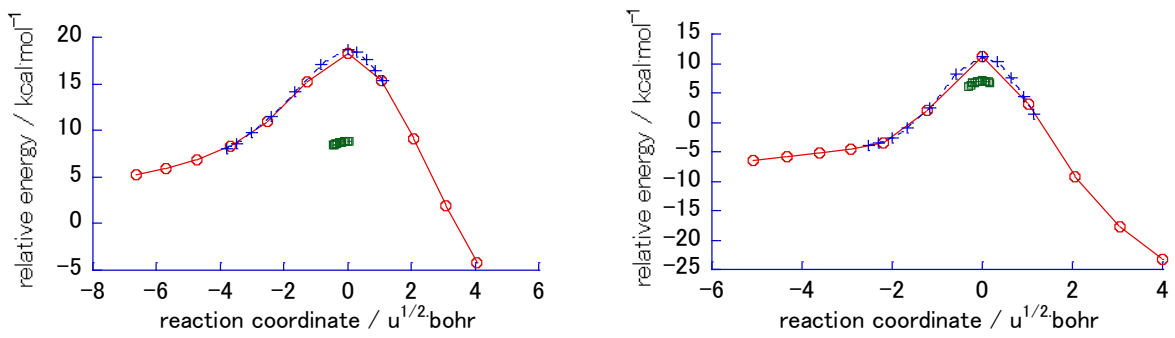

Fig. 4. Optimized reaction pathway obtained by using the CI and CEI approaches. The red line with circle and the blue dotted line with cross symbols show the results of CI and CEI, respectively, after 100 optimization cycles using the quick-min optimization algorithm. The green lines show relative energies of images after 1150 and 1500 cycles for TS1 and TS2, respectively by using the CEI approach. The relative energies for a) TS1 and b) TS2 based on the reactant energy are shown.

Then, the CEI calculations were continued by 1500 optimization cycles. Since these optimization cycles may require restarting jobs from previously obtained unconverged structures by the GAMESS program, the input file for restarting the

optimization is also provided in the supplementary material. The convergence threshold used in this calculation was 0.1 kcal/mol·Å, 10.0 kcal/mol·Å, 0.01 Å, and 0.1 Å for the root mean square (RMS) forces, maximum forces, RMS displacement, and maximum displacement of atoms, respectively. Although the thresholds were satisfied for TS1 after 1150 steps, RMS forces for TS2 did not satisfy the threshold even at 1500 steps. At these point, the images with the highest energy have maximum forces on atoms of 0.209 and 0.224 kcal/mol·Å for TS1 and TS2, respectively, which are equivalent with 0.00907 and 0.00971 eV/ Å. The relative energies at both TSs decreased with an increasing number of optimization cycles; this is reasonable because the TS structures are saddle points between two stable structures, and the unconverged pathway should pass through higher energy regions. To determine the reliability of the obtained TS structures using the CEI algorithm, the TS structures were also evaluated by using analytical second derivative techniques as illustrated in Fig. 5. The relative energies at TS1 and TS2 were found to be 8.6 and 7.0 kcal/mol, respectively, based on the reactant using the second derivatives. These values were in good agreement with 8.8 and 7.0 kcal/mol, respectively, obtained by the CEI approach. The maximum difference in interatomic distances was 0.04 Å and less than 0.01 Å for TS1 and TS2, respectively. These results confirmed that the CEI approach should be useful for obtaining TS structures even though the reliable Hessians could not be evaluated

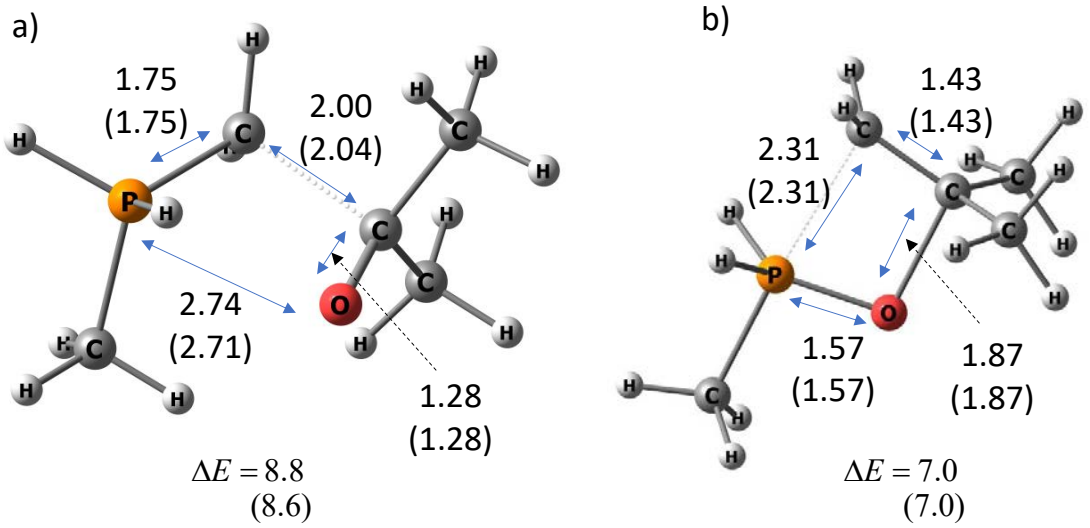

Fig. 5. Optimized structures of TS1 and TS2 evaluated by using hessians and the CEI approaches. The values are interatomic distances given in Å. The relative energies based on the reactant, ΔE, are also presented in kcal/mol. The results of using Hessians on (a) TS1 and (b) TS2 are compared with the results in paranthesis of using the CEI approach. The imaginary frequencies using Hessians of (a) and (b) are *i*329.7 cm^{-1} and *i*547.0 cm^{-1}, respectively.

by such as the coupled cluster molecular orbital calculations and/or the free-energy-gradient molecular dynamics simulations [4–6,22].

The calculated overall reaction pathway of the Wittig reaction is depicted in Fig. 6. The reactant composed of non-stabilized ylide and acetone can produce the intermediate IM in vacuum via the energy barrier of 8.6 kcal/mol, and the reverse energy barrier is high to be 22.9 kcal/mol. The intermediate structure IM is known as the oxaphosphetane intermediate, which is stable with an activation barrier of 21.3 kcal/mol to generate the product by releasing the phosphine oxide. Because the energy barrier of the reverse reaction from the product to IM is very high (42.0 kcal/mol), it is difficult to occur reversible reaction for this system.

The convergence profile of the maximum root mean square (MRMS) forces in all images using the CEI approach are shown in Fig. 7. For the TS1 optimization, the MRMS forces gradually decreased to converge. In contrast, the MRMS forces

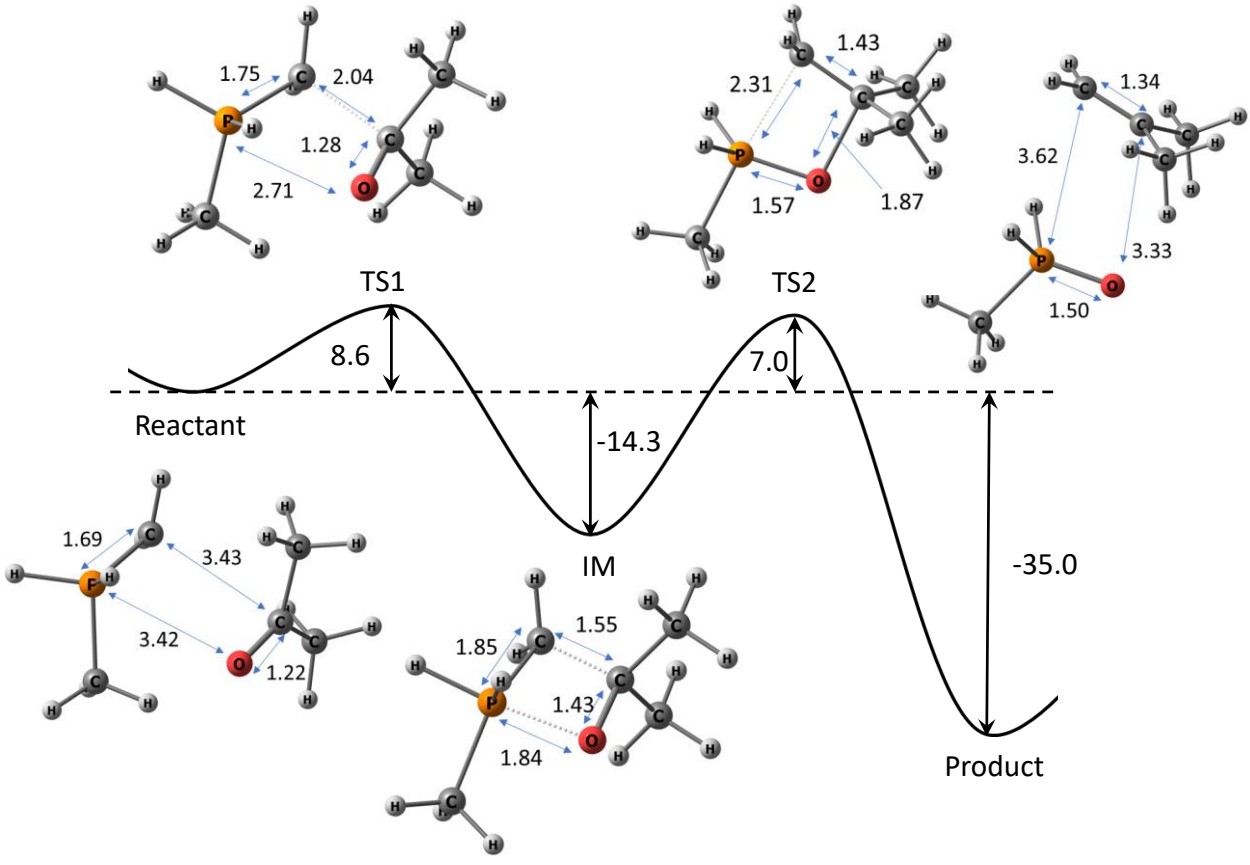

Fig. 6. Overall reaction pathway of the Wittig reaction considered in this study. The structures and energies in this figure were fully optimized by B3LYP/6-311++G(d,p) with dispersion correction. The interatomic distances and relative energies are expressed in Å and kcal/mol, respectively.

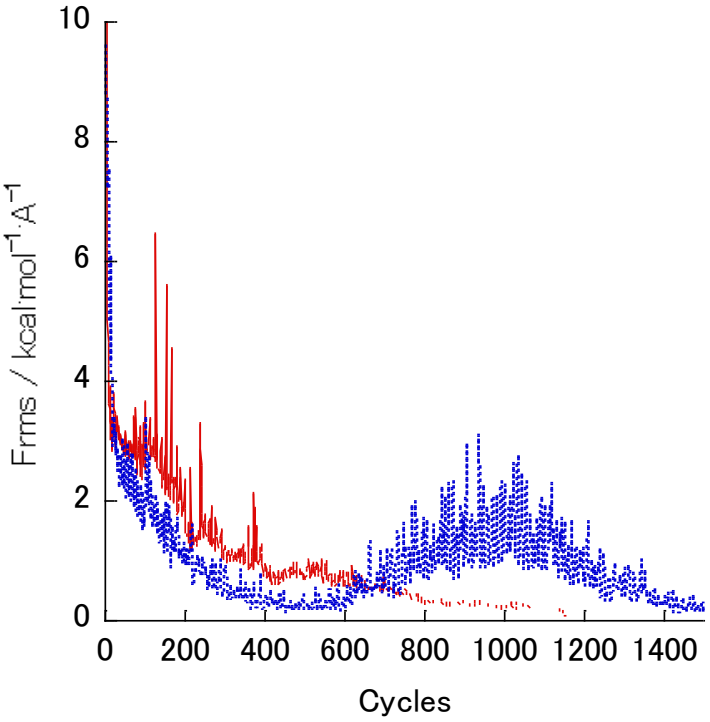

Fig. 7. Convergence of forces during the optimization process. MRMS forces in all images are indicated. Red solid line represents the result of images for optimizing TS1. Blue broken line shows the results of optimizing TS2 by 1500 cycles.

decreased to 0.446 kcal/mol·Å at 450 optimization cycles for the TS2 optimization; it increased over 1000 cycles owing to the existence of the flat potential region between IM and the product. In TS2 at 450 cycles, the rotational angle of one of the methyl groups differed from that shown in Fig. 5(b) by 53.7 degree. In contrast, the interatomic distances were close to those depicted in Fig. 5(b). This implies that the low MRMS force at 450 cycles for TS2 optimization originated from the flat potential region because of the methyl group rotation. The parallel and perpendicular components of the maximum force on atoms at the image with the highest energy were also depicted in the supplementary Figure S1. The parallel component along the elastic band are not dominant and the perpendicular components are dominant during the optimization as seen in Figure S1.

The CEI approach successfully obtained the TS structures using only the gradients of the energy surface without evaluating Hessians. Because all images could climb toward the TS structures by specifying small value of λ in Eq.4, only a few images were sufficient to obtain the TS structure, thereby saving computational resources.

4. Conclusion

The CEI algorithm based on the NEB approach was proposed to obtain TS structures. This approach was implemented in the GAMESS program. According to this algorithm, the end images, which are terminal structures in the chain of states representing the reaction pathway, were optimized to climb to the TS along the reaction path using the inverse parallel component of forces acting on atoms. In addition, the distance between adjacent images can be shorten by applying a small values of λ in Eq.4. The algorithm was applied to the simplified Wittig reaction to analyze the behavior during the optimization procedure. As the number of optimization cycles increased, all the structures of the images could successfully approach the TS region, and the density of images in the TS region gradually increased. This also results that the tangent vector of the reaction pathway increases the reliability because the tangent vector is approximated by the direction connecting adjacent discretized images.

Because only the gradients of the potential surface are required, the CEI algorithm should be useful for obtaining TS structures even though the reliable Hessians could not be evaluated by employing such as the coupled cluster method and/or the free-energy-gradient molecular dynamics simulations under thermal equilibrium conditions. Although many optimization cycles are currently required to obtain the TS structures by the quick-min algorithm, more efficient optimization techniques suitable for NEB approaches can reduce the optimization cycles.

Acknowledgement

This work was supported by Grant-in-Aid for Scientific Research (C) from the Japanese Ministry of Education, Culture, Sports, Science and Technology (No. JP19K05375, JP20H02716 and JP20K21007). We would like to thank Editage (www.editage.com) for English language editing.

References

[1] Abramowitz, M. and Stegun, I. A. (Eds.). Handbook of Mathematical Functions with Formulas, Graphs, and Mathematical Tables, 9th printing. New York: Dover, p. 18, 1972.

[2] Kelley, C.T. Iterative Methods for Optimization, Society for Industrial and Applied Mathematics, Philadelphia: SIAM, p.71, 1999.

[3] M. Nagaoka, N. Okuyama-Yoshida and T. Yamabe, Origin of the Transition State on the Free Energy Surface: Intramolecular Proton Transfer Reaction of Glycine in Aqueous Solution, *J. Phys. Chem. A*, 1998, 102, 8202–8208.

[4] T. Asada, K. Ando, K. Sakurai, S. Koseki, M.Nagaoka, Efficient approach to include molecular polarizations using charge and atom dipole response kernels to calculate free energy gradients in the QM/MM scheme, *Phys. Chem. Chem. Phys.*, 2015, 17, 26955-26968.

[5] T. Asada, K. Ando, P. Bandyopadhyay, S. Koseki, Free energy contribution analysis using response kernel approximation: insights into the acylation reaction of a beta-lactamase, *J. Phys. Chem. B.*, 2016, 120, 9338–9346.

[6] T. Asada, P. Bandyopadhyay, and S. Koseki, Computational Approach for Molecular Design Using Free Energy Contrubution Analysis, *AIP Conference Proceedings*, 2018, 2040, 020016.

[7] G. Mills, H. Jónsson, Quantum and thermal effects in H_2 dissociative adsorption: evaluation of free energy barriers in multidimensional quantum systems, *Phys. Rev. Lett.* 1994, 72, 1124–1127.

[8] G. Mills, H. Jónsson, G.K. Schenter, Reversible work transition state theory: application to dissociative adsorption of hydrogen, *Surf. Sci.*, 1995, 324, 305–337.

[9] H. Jónsson, G. Mills, K.W. Jacobsen, Nudged elastic band method for finding minimum energy paths of transitions, *Class. Quantum Dyn. Condens. Phase Simulations*, 1998, 385–404.

[10] E.W., W. Ren, E. Vanden-Eijnden, String method for the study of rare events, *Phys. Rev. B*, 2002, 66, 52301.

[11] T. Asada, N. Sawada, T. Nishikawa, and S. Koseki, An improved reaction path optimization method using a chain of conformations, *Chem. Phys. Lett.*, 2018, 699, 255-260.

[16] Maragakis, P.; Andreev, S. A.; Brumer, Y.; Reichman, D. R.; Kaxiras, E. Adaptive Nudged Elastic Band Approach for Transition State Calculation. *J. Chem. Phys.*, 2002, 117, 4651–4658.

[13] M.W.Schmidt, K.K.Baldridge, J.A.Boatz, S.T.Elbert, M.S.Gordon, J.H.Jensen, S.Koseki, N.Matsunaga, K.A.Nguyen, S.Su, T.L.Windus, M.Dupuis, J.A.Montgomery, General Atomic and Molecular Electronic Structure System, *J. Comput. Chem.*, 1993, 14, 1347-1363.

[14] G. Wittig, U. Schöllopf, Über Triphenyl‐phosphin‐methylene als olefinbildende Reagenzien (I. Mitteil.), *Chem. ber.*, 1954, 87, 1318-1330.

[15] G. Wittig, W. Haag, Über Triphenyl‐phosphinmethylene als olefinbildende Reagenzien (II. Mitteil.), *Chem. ber.*, 1955, 88, 1654-1666.

[16] Smidstrup, S.; Pedersen, A.; Stokbro, K.; Jónsson, H. Improved Initial Guess for Minimum Energy Path Calculations, *J. Chem. Phys.*, 2014, 140, 214106.

[17] Henkelman, G.; Jónsson, H. Improved Tangent Estimate in the Nudged Elastic Band Method for Finding Minimum Energy Paths and Saddle Points, *J. Chem. Phys.,* 2000, 113, 9978–9985.

[18] Henkelman, G.; Uberuaga, B. P.; Jónsson, H. A Climbing Image Nudged Elastic Band Method for Finding Saddle Points and Minimum Energy Paths, *J. Chem. Phys.*, 2000, 113 (22), 9901–9904.

[19] Herbol, H. C.; Stevenson, J.; Clancy, P. Computational Implementation of Nudged Elastic Band, Rigid Rotation, and Corresponding Force Optimization, *J. Chem. Theory Comput.*, 2017, 13, 3250–3259.

[20] Sheppard, D.; Terrell, R.; Henkelman, G. Optimization Methods for Finding Minimum Energy Paths, *J. Chem. Phys.*,

2008, 128, 134106.
[21] Bitzek, E.; Koskinen, P.; Fähler, F.; Moseler, M.; Gumbsch, P. Structural relaxation made simple, *Phys.Rev.Lett.*, 2006, 97, 170201.
[22] Hu, H.; Lu, Z.; Parks, J.M.; Burger, S.K.; Yang, W. Quantum mechanics/molecular mechanics minimum free-energy path for accurate reaction energetics in solution and enzymes: Sequential sampling and optimization on the potential of mean force surface, *J. Chem. Phys.*, 2008, 128, 034105.